# Coherent structures and self-consistent transport in a mean field Hamiltonian model

D. del-Castillo-Negrete*

*Oak Ridge National Laboratory*

*Oak Ridge TN, 37831-8071*

Marie-Christine Firpo

*Dipartimento di energetica "Sergio Stecco",*

*Università degli studi di Firenze,*

*Via Santa Marta, 3, I-50139 Firenze*

## Abstract

A study of coherent structures and self-consistent transport is presented in the context of a Hamiltonian mean field, single wave model. The model describes the weakly nonlinear dynamics of marginally stable plasmas and fluids, and it is related to models of systems with long–range interactions in statistical mechanics. In plasma physics the model applies to the interaction of electron "holes" and electron "clumps", which are depletions and excesses of phase-space electron density with respect to a fixed background. In fluid dynamics the system describes the interaction of vortices with positive and negative circulation in a two-dimensional background shear flow. Numerical simulations in the finite–$N$ and in the $N \to \infty$ kinetic limit (where $N$ is the number of particles) show the existence of coherent, rotating dipole states. We approximate the dipole as two "macroparticles" (one hole and one clump)

*e-mail: delcastillod@ornl.gov

and consider the $N = 2$ limit of the model. We show that this limit has a family of symmetric, rotating integrable solutions described by a one-degree-of-freedom nontwist Hamiltonian. A perturbative solution of the nontwist Hamiltonian provides an accurate description of the mean field and rotation period of the dipole. The coherence of the dipole is explained in terms of a parametric resonance between the rotation frequency of the macroparticles and the oscillation frequency of the self-consistent mean field. This resonance creates islands of integrability that shield the dipole from regions of chaotic transport. For a class of initial conditions, the mean field exhibits an elliptic–hyperbolic bifurcation that leads to the filamentation, chaotic mixing and eventual destruction of the dipole.

**The study of active transport deals with the problem of interacting tracers. This interaction can be of two types: Tracers can interact among themselves, as in the case of the advection of chemical or biological species, or with the advecting field. In the latter case, the advecting field is determined by the tracer. An example of this type of transport, also known as self-consistent transport, is an ensemble of charged particles when the self-generated electric field of the particles is taken into account, other examples include point vortices in fluid dynamics and the transport of gravitational interacting particles. A convenient approach in the study of this type of self-consistent transport problems is the use of mean field models. In these models the interacting tracers are treated as independent tracers moving in an effective field determined self-consistently from the tracers. Since the early studies on chaotic transport, the study of transport by waves has been a problem of interest in fluid dynamics and plasma physics. A relatively well-understood problem is the study of passive transport in the presence of given, time dependent waves. Less studied is the problem of active transport by waves. In this paper we study this problem in the context of**

**the single wave model, which is a mean field Hamiltonian model describing the dynamics of marginally stable fluids and plasmas. In the single wave model the self-consistent interaction between the wave and the tracer is incorporated in a time–modulation of the wave amplitude. Our specific objective is to understand the role of chaotic transport and self-consistent dynamics in the formation and destruction of coherent structures.**

## I. INTRODUCTION

The study of transport in Hamiltonian systems is important because of its intrinsic interest in nonlinear dynamics and its applications to fluid mechanics, plasmas physics, and statistical mechanics. In a two-dimensional phase space, the problem is to determine the evolution of an ensemble of $N$ initial conditions $(x_j(0), u_j(0))$ such that

$$\frac{dx_j}{dt} = \frac{\partial H}{\partial u_j}\,, \qquad \frac{du_j}{dt} = -\frac{\partial H}{\partial x_j}\,, \tag{1}$$

where $H$ is the Hamiltonian of the system, and the index $j = 1, 2, \ldots N$ is a particle label. Depending on the Hamiltonian, one can distinguish two different transport problems: *passive transport* and *active transport*. In a passive transport problem, the Hamiltonian is given, and it does not depend on the dynamics of the particles. However, in an active transport problem, the Hamiltonian is determined by the dynamics of the particles.

The study of transport of passive scalars in a two–dimensional, incompressible fluid is a typical example of a Hamiltonian passive transport problem. In this case, the fluid dynamics streamfunction plays the role of Hamiltonian, and the $(x_j, y_j)$ spatial coordinates of the passive tracers correspond to the canonical phase space coordinates $(x_j, u_j)$. Another example of passive transport is the study of "test" charged particles in an external electrostatic field in plasma physics. In this case, one refers to "test" particles to stress the fact that the electric field created by the particles is neglected.

An example of an active transport problem is the transport of an ensemble of charged particles in the case when the self-generated electric field of the particles, rather than being neglected, is taken into account in addition to the external field. Another example is an ensemble of gravitational interacting particles, a problem of interest to galactic dynamics. In fluid dynamics, the transport of mutually interacting point vortices is also an active transport problem. Active transport is also called self-consistent transport because the Hamiltonian of the system is determined by a self-consistency relation between the particles and the fields. This relation is Poisson's equation in the plasma physics and galactic dynamics context, and the vorticity–streamfunction relation in the fluid dynamics context.

Passive transport in two dimensions has been extensively studied in the literature, see for example Ref. [1] and references therein. This problem reduces to the study of the dynamics of one-degree-of-freedom, time-dependent Hamiltonian systems. The case of periodic time dependence is particularly well-understood. The problem of self-consistent transport is in general a more demanding task and much less is known about it. In Refs. [2,3] the use of mean field models was proposed to address this problem. The idea of the mean field approach is to treat the interacting particles as independent particles moving in an average potential determined self-consistently from the motions of all the particles. In this approach, the equations governing the motion of N interacting particles reduce to the equation governing the motion of a single particle under an effective potential. That is, the only influence a particle has in the rest is through its contribution to the effective potential. Mean field transport models lay between the relatively easy to understand but limited passive transport models and the complex many–body self-consistent transport models.

The mean field model of interest here is the *single wave model* according to which the dynamics evolves according to Eq. (1) with

$$H = \sum_{j=1}^{N} \left[ \frac{1}{2}\, u_j^2 - a(t)\, e^{ix_j} - a^*(t)\, e^{-ix_j} \right] , \tag{2}$$

which is the Hamiltonian of an ensemble of $N$ particles in the field of a time-dependent wave with a single harmonic with wave-number $k = 1$. The nontrivial aspect of the model is in the mean field $a(t)$, which is determined by the self-consistency relationship

$$\frac{da}{dt} - iUa = \frac{i}{N} \sum_{j=1}^{N} \Gamma_j\, e^{-ix_j} \ , \tag{3}$$

where $U$ and $\Gamma_j$ are constants. The parameter $U$ is the wave frequency in the absence of particles and is of the order of the plasma frequency for plasmas. The parameters $\Gamma_j$ are usually taken positive (e.g., Refs. [4–7]). However, following the generalization of the single wave model discussed in Refs. [2,3,8,9], we consider here the case in which these parameters can be positive or negative.

In the kinetic limit ($N \to \infty$), the Hamiltonian transport problem in Eq. (1) is described by a phase distribution function $f$, evolving according to the Liouville equation

$$\partial_t f + \partial_u H \; \partial_x f - \partial_x H \, \partial_u f \; = 0 \, . \tag{4}$$

As before, one can distinguish in this case between passive transport and self-consistent transport. In the first case, $H$ is a given function of $x$, $u$ and $t$, and Eq. (4) is a linear equation. However, in the self-consistent case, $H$ depends on $f$ through a self-consistent condition. In the single wave model:

$$H = \frac{u^2}{2} - a(t)\, e^{i\, x} - a^*(t)\, e^{-i\, x} \, , \qquad \frac{da}{dt} - iUa = \frac{i}{2\pi} \int e^{-ix}\, dx \int du\, f \, . \tag{5}$$

The single wave model has its origins in the study of the beam-plasma instability in plasma physics [4–6]. More recently, the model has been derived under more general conditions, and its range of applicability considerably expanded. In Ref. [7] the mean field–particle Lagrangian of the model was derived from the full N-body classical mechanics Lagrangian for Coulomb interactions. In Refs. [8,9] a derivation of the single wave model in the context of kinetic theory was presented using matched asymptotic expansions, and it was shown that the model provides a universal description of the weakly nonlinear dynamics of marginally stable plasmas and fluids. Single wave models have also been used in the study of free electron lasers [10], finite-amplitude non-axisymmetric perturbation of vortices [11], and critical layer dynamics in shear flows [12–14]. There are also similarities between the single wave model and models used in the study of systems with long-range interactions in statistical mechanics [15,16].

The single wave model in Eqs. (4) and (5) describes the dynamics of localized perturbations. Depending on their sign, perturbations are classified as clumps and holes. Clumps correspond to $f > 0$ and represent perturbations that increase the equilibrium distribution. Holes correspond to $f < 0$ and represent depletions of the equilibrium distribution [8,9]. For finite $N$,

$$f(x,u,t) = \frac{2\pi}{N} \sum_{j=1}^{N} \Gamma_j \, \delta[x - x_j(t)] \, \delta[u - u_j(t)] \; , \tag{6}$$

and particles with $\Gamma_j > 0$ correspond to clumps, and those with $\Gamma_j < 0$ correspond to holes. The formation of holes and clumps in the nonlinearly saturated state of plasma kinetic

instabilities in a dissipative medium has been studied in Ref. [17]. In fluid dynamics, the interaction of vorticity clumps and vorticity holes with a background vorticity gradient was considered in Ref. [18]. Here we present a study of holes and clumps in the context of the single wave model. In particular, we focus on the formation and destruction of coherent rotating dipole states. Because of the generality of the single wave model, we expect the results discussed here to be relevant to plasmas and fluids. Also, the idea of allowing the sign of the $\Gamma_j$ parameters to change, might have interesting implications in the context of mean field coupled rotators models in statistical mechanics.

The organization of the rest of the paper is as follows. In Sec. II we present numerical solutions of coherent, rotating dipole states in the finite–$N$ limit, and in the $N \to \infty$ kinetic limit. We describe these solutions as two macroparticles (one hole and one clump) and study the $N = 2$ limit of the model. Section III presents a perturbative solution of the $N = 2$ model and describes the mean field-dipole resonance. This resonance explains the robustness of the dipole state and clarifies the connection between self-consistent chaos and coherent structures. In Sec. IV we discuss an elliptic–hyperbolic bifurcation that leads to the destruction of dipole states and to phase space mixing. The conclusions are presented in Sect. V.

## II. COHERENT, ROTATING DIPOLE STATES

The spontaneous formation of coherent structures has been observed in numerical simulations and laboratory experiments in fluids and plasmas, see for example Ref. [19,20] and references therein. Phase space "clustering" has also been observed in mean field models of systems with long range interactions [15,21]. These structures typically coexist in a turbulent background, and a problem of interest is to explain their coherence against the chaotic advection induced by the background. In this section we explore this problem in the context of the single wave model.

Figure 1 shows an example of a coherent, rotating dipole in the kinetic ($N \to \infty$) limit,

obtained by integrating numerically Eqs. (4)–(5) with periodic boundary conditions in $x$, $f \to 0$ as $u \to \pm\infty$, and initial condition

$$f(x, u, t = 0) = f_1 - f_2 \,, \qquad a(t = 0) = a_0 \,, \tag{7}$$

where

$$f_j = \gamma \, \exp\left[ - \left( \frac{x - x_j}{\sigma_x} \right)^2 - \left( \frac{u - u_j}{\sigma_u} \right)^2 \right] , \tag{8}$$

with $\gamma = 5$, $x_1 = x_2 = \pi$, $u_1 = -u_2 = 0.4$, $a_0 = -0.2$, $\sigma_x = 0.2$, $\sigma_u = 0.1$, and $U = 0$. For the numerical integration we used an operator splitting scheme [22], spectral in $x$ and finite difference with cubic splines interpolation in $u$. Figure 2 shows the corresponding time periodic dependence of the real part of the mean field $a(t)$. Because Eqs. (4)–(5) are invariant under the symmetry transformation $(x, u, f, a) \to (-x + 2\pi, -u, -f, a^*)$ for $U = 0$, symmetric initial states like the one in Eqs. (7)–(8) remain symmetric and the imaginary part of $a$ vanishes for all $t$.

The relationship between kinetic simulations and finite–$N$ particle simulations is not trivial. In particular, kinetic simulations inevitably introduce some sort of numerical dissipation. In addition, as discussed in Refs. [23–25], if the limits $t \to \infty$ and $N \to \infty$ do not commute, there might be discrepancies in the long–time limit. As a first step to address these issues we performed finite–$N$ numerical simulation of the single wave model in Eqs. (1)–(3) using a fourth-order symplectic algorithm [26]. Figure 3 shows an $N = 1000$ (half holes and half clumps) simulation of a coherent rotating dipole with $U = 0$ and $a(t = 0) = -0.2$. The initial conditions of the particles and the $\Gamma_j$'s were chosen according to a finite–$N$ discretization of $f(x, u, t = 0)$ in Eqs. (7)–(8) with the same energy and momentum as the kinetic simulation in Fig. 1. Consistent with the kinetic result, the finite–$N$ dipole rotates maintaining its coherence. A plot of the mean field $a$ over one rotation period shown in Figure 4, indicates that the finite–$N$ result (dashed line) lags slightly behind the kinetic result (solid line). This might indicate a possible finite–$N$ dependence of the dipole rotation frequency. The circles in this plot are the $N = 2$, macroparticle analytical result to be discussed in

Sec. III-A. Preliminary results indicate that finite–$N$ effects might also be present in the long-time modulation of the oscillating mean field $a$.

The rotating dipole can be viewed, in a first approximation, as two "macroparticles" rotating around the $(x, u) = (\pi, 0)$ equilibrium fixed point. Based on this idea, we focus in the $N = 2$ case of the single wave model. Equations (1)–(3) are invariant with respect to the transformation $(x_j, u_j, \Gamma_j, a) \to (-x_j, -u_j, -\Gamma_j, a^*)$ provided $U = 0$. Motivated by this result we consider two-particles ($N = 2$) symmetric solutions consisting of one clump and one hole with $\Gamma_1 = -\Gamma_2 = \Gamma$, $U = 0$, and symmetric initial conditions $x_1(0) = -x_2(0)$, $u_1(0) = -u_2(0)$, and $a(0) = a^*(0)$. Substituting $x_1(t) = -x_2(t) = x(t)$, $u_1(t) = -u_2(t) = u(t)$, and $a(t) = a^*(t)$ into Eqs. (1)–(3), we get:

$$\frac{dx}{dt} = u \tag{9}$$

$$\frac{du}{dt} = -2\, a \sin x \tag{10}$$

$$\frac{da}{dt} = \Gamma \sin x\,. \tag{11}$$

Thus, whereas the phase space of a general $N = 2$ system is six-dimensional, the phase space of a symmetric hole-clump configuration is three-dimensional, and the dynamics is determined by the real function $a(t)$ and the state $(x, u)$ of one of the particles. The system in Eqs. (9)–(11) can be further reduced using conservation laws. There are two conserved quantities in the single wave model, the momentum $\mathcal{P}$ and the energy $\mathcal{E}$ defined as

$$\mathcal{P} = \frac{1}{N}\sum_{j=1}^{N} \Gamma_j\ u_j + |a|^2 \tag{12}$$

$$\mathcal{E} = \frac{1}{N}\sum_{j=1}^{N} \Gamma_j \left( \frac{u_j^2}{2} - a\, e^{i x_j} - a^*\, e^{-i x_j} \right) - U\,|a|^2\,. \tag{13}$$

For a symmetric system

$$\mathcal{P} = \Gamma u + a^2\,, \tag{14}$$

and $\mathcal{E} = 0$.

Equation (14) allows the reduction of Eqs. (9)–(11) to the one-degree-of-freedom Hamiltonian system

$$\frac{dx}{d\tau} = \frac{\partial H}{\partial A}\,, \qquad \frac{dA}{d\tau} = -\frac{\partial H}{\partial x}\,, \tag{15}$$

with

$$H = \alpha\, A - \frac{A^3}{3} + \cos x\,, \tag{16}$$

where we have introduced the rescaled variables:

$$A = a\Gamma^{-2/3}\,, \qquad \tau = \Gamma^{1/3}\, t\,, \qquad \alpha = \mathcal{P}\Gamma^{-4/3}\,. \tag{17}$$

Being time independent, the Hamiltonian system in Eqs. (15)-(16) is completely integrable. In Ref. [6] it was shown that the single wave model with one particle is integrable. Here we add to this integrable solution a new one consisting of two symmetrically located particles. Once $A$ and $x$ are found, $u$ is determined from Eq. (14) according to

$$u = \frac{\mathcal{P}}{\Gamma}\left(1 - \frac{A^2}{\alpha}\right)\,. \tag{18}$$

Because of the cubic dependence on $A$, the Hamiltonian in Eq. (16) is a *nontwist Hamiltonian* [27]. Nontwist Hamiltonians are degenerate Hamiltonians for which the frequency, $\partial_J H$, is not a monotonic function of the action $J$. These Hamiltonians appear in the study of transport in nonmonotonic shear flows (jets) and in the study of stochasticity of magnetic field lines in plasmas with nonmonotonic $q$ profiles [28]. From the dynamical systems point of view, nontwist Hamiltonians are interesting because several well-known results, including the KAM theorem and the Poincare-Birkhoff theorem, can not be applied to them (for further discussion on nontwist systems see Ref. [27] and references therein.)

When $\alpha < 0$ the system in Eq. (15) has no fixed points, and when $\alpha > 0$ the system has four fixed points: $(x_0, A_0) = (0, \sqrt{\alpha})$ , $(0, -\sqrt{\alpha})$, $(\pi, \sqrt{\alpha})$, and $(\pi, -\sqrt{\alpha})$, with eigenvalues $\lambda = \pm i\omega$, $\lambda = \pm\omega$, $\lambda = \pm\omega$, and $\lambda = \pm i\omega$, respectively, where

$$\omega = \sqrt{2}\,\alpha^{1/4}\,. \tag{19}$$

That is, the elliptic and hyperbolic fixed points come in pairs. The value $\alpha = 0$ is the bifurcation point at which an elliptic–hyperbolic doublet is created at $x = 0$, and another

elliptic–hyperbolic doublet is created at $x = \pm\pi$. The symmetry in the stability properties of the fixed point is related to the symmetry $(x_j, a) \to (x_j + \pi, -a)$ of the single wave model.

A generic property of nontwist Hamiltonians like the one in Eq. (16) is that they exhibit separatrix reconnection, which involves the different ways in which the stable and unstable manifolds of the hyperbolic fixed points can be connected [27]. The reconnection threshold can be computed by observing that at the reconnection point, $H(P_0) = H(P_\pi)$, where $H$ is the Hamiltonian in Eq. (16), $P_0 = (0, -\sqrt{\alpha})$ and $P_\pi = (\pi, \sqrt{\alpha})$. This condition gives the reconnection threshold $\alpha_* = (3/2)^{2/3}$. For $\alpha < \alpha_*$ the Hamiltonian has an homoclinic topology, and for $\alpha > \alpha_*$ it has an heteroclinic topology. The difference between these topologies is illustrated in Fig. 5. Panel (a) shows the homoclinic topology with $\alpha = 0.5$ and panel (b) the heteroclinic topology with $\alpha = 1.95$. Since the Hamiltonian in Eq. (16) is time independent, the orbits of the system in Eqs. (9)–(11) correspond to contours of constant $H$ in Fig. 5.

These $N = 2$ results can be used to interpret the kinetic simulations. To do this, we define the "effective"$\Gamma$ and momentum $\mathcal{P}$ for the kinetic initial condition in Eqs. (7)–(8) as

$$\Gamma = \frac{1}{\pi}\int\int f_1 \, dxdu = \gamma\,\sigma_x\sigma_u\,, \qquad \mathcal{P} = \frac{1}{2\,\pi}\int\int f\,u\,dxdu \; + |a|^2 = \gamma\,u_1\sigma_x\sigma_u + |a_0|^2\,. \quad (20)$$

According to Eqs. (17) and (19), the linear approximation of the rotation period (in dimensional units) is $T = \sqrt{2}\,\pi/\mathcal{P}^{1/4}$ where $\mathcal{P}$ is the momentum of the system. Treating the kinetic dipole in Fig. 1 as two macroparticles with the same momentum we obtain the following approximation for the rotation period:

$$T = \frac{\sqrt{2}\,\pi}{\mathcal{P}^{1/4}} = \frac{\sqrt{2}\,\pi}{\left(\gamma\,u_1\sigma_x\sigma_u + |a_0|^2\right)^{1/4}}\,. \quad (21)$$

For the parameter values used in the kinetic simulation, Eq. (21) gives $T = 8.35$ close to the period $T = 8.66$ according to Fig. 2. In Sec. III-A a second order correction to this linear estimate is presented. Using Eqs. (20), the value of $\alpha = \mathcal{P}\Gamma^{-4/3}$ can be computed, and the topology of the reduced nontwist Hamiltonian of the macroparticles determined. In particular, for the kinetic simulation in Fig. 1, $\alpha = 1.7235 > \alpha_*$, which corresponds to the heteroclinic topology.

## III. MEAN FIELD–DIPOLE RESONANCE

In the previous section it was shown that the $N = 2$ hole-clump, symmetric system is integrable. As observed in Fig. 5, in the $(x, A)$ phase space there are trapped orbits and untrapped orbits. These two types of orbits are divided by the separatrix. In this section we focus on the trapped orbits. In particular, we consider perturbative solutions of the symmetric dipole system in Eq. (15) in the vicinity of the equilibrium elliptic point $(x_0, A_0) = (0, \sqrt{\alpha})$. From the dynamical point of view, this calculation describes a linear nontwist oscillator in the $(x, A)$ variables.

### A. Nontwist oscillator

Approximating $\sin x \approx x - x^3/6$, and writing

$$A = \sqrt{\alpha} - \varepsilon\,\omega^2\,\phi\,, \qquad x = \varepsilon\,\omega^3\,\psi\,, \qquad T = \omega\tau\,, \qquad \omega^2 = 2\,\sqrt{\alpha}\,, \tag{22}$$

Eq. (15) becomes

$$\frac{d\phi}{dT} = -\psi + 2\,\lambda\,\varepsilon^2\,\psi^3\,, \tag{23}$$

$$\frac{d\psi}{dT} = \phi - \varepsilon\,\phi^2\,, \tag{24}$$

with

$$\phi(0) = 1\,, \qquad \psi(0) = 0\,, \qquad \varepsilon = \frac{\sqrt{\alpha} - A(0)}{\omega^2}\,, \qquad \lambda = \left(\frac{\alpha}{\alpha_*}\right)^{3/2}\,, \tag{25}$$

where $\alpha_* = (3/2)^{2/3}$ is the separatrix reconnection threshold. We assume that $\varepsilon \ll 1$ and write

$$\phi = \phi_0 + \varepsilon\,\phi_1 + \ldots\,, \qquad \psi = \psi_0 + \varepsilon\,\psi_1 + \ldots\,. \tag{26}$$

Substituting Eq. (26) into Eqs. (23) and (24), it is observed that the perturbation series leads to secular growth at second order in $\varepsilon$. This motivates the introduction of the *slow*

*time variable* $\eta = \varepsilon^2 T$. Treating $\phi$ and $\psi$ as functions of these two variables we have $d_T \to \partial_T + \varepsilon^2 \partial_\eta$, and

$$\frac{\partial \phi}{\partial T} + \varepsilon^2 \frac{\partial \phi}{\partial \eta} = -\psi + 2\lambda \varepsilon^2 \psi^3 \ , \tag{27}$$

$$\frac{\partial \psi}{\partial T} + \varepsilon^2 \frac{\partial \psi}{\partial \eta} = \phi - \varepsilon \psi^2 \, . \tag{28}$$

The solutions to zeroth and first order are given by

$$\phi_0 = C\, e^{i\,T} + C^*\, e^{-i\,T} \, , \qquad \phi_1 = 2\, CC^* \, - \frac{1}{3} \cos T - \frac{C^2}{3}\, e^{2i\,T} - \frac{C^{*2}}{3}\, e^{-2i\,T} \, , \tag{29}$$

where $C = C(\eta)$, and $\psi_k = -\partial_T \phi_k$ for $k = 0$ and 1. To second order

$$\frac{\partial^2 \phi_2}{\partial T^2} \, + \phi_2 \, = -2\, e^{i\,T} \left( i\, \frac{dC}{d\eta} - \frac{5}{3}\, C^2 C^* - 3\, \lambda\, C^2\, C^* \right) + \text{c.c.} + \text{NR} \, , \tag{30}$$

where c.c. denotes the complex conjugate, and $NR$ denotes all the nonresonant terms. That is, terms of the form $e^{imT}$ with $m \neq \pm 1$. To avoid secular growth, we kill the resonant term on the right-hand side by choosing $C$ such that

$$i\, \frac{dC}{d\eta} = \left( \frac{5}{3} + 3\, \lambda \right) \, C^2 C^* \, , \tag{31}$$

that is

$$C = \rho_0 \, \exp \, i \left[ \theta_0 - \left( \frac{5}{3} + 3\, \lambda \right) \, \rho_0^2 \, \eta \right] \, , \tag{32}$$

where $\rho_0$ and $\theta_0$ are integration constants. Choosing $\rho_0 = 1/2$ and $\theta_0 = 0$ gives the desired initial condition $\phi(0) = 1$, $\psi(0) = 0$, and we conclude from (22), (29) and (32)

$$A(\tau) = \frac{\omega^2}{2} \left[ 1 - 2\, \varepsilon \, \cos \Omega\, \tau - \varepsilon^2 \left( 1 - \frac{2}{3} \, \cos \Omega \tau - \frac{1}{3} \, \cos 2\, \Omega\, \tau \right) \right] \, , \tag{33}$$

$$x(\tau) = \omega^3 \, \left[ \varepsilon \, \sin \Omega\, \tau - \frac{\varepsilon^2}{3} \left( \sin \Omega\, \tau + \sin 2\, \Omega\, \tau \right) \right] \, , \tag{34}$$

where we have defined

$$\Omega = \left[ 1 - \left( \frac{5 + 9\lambda}{12} \right) \, \varepsilon^2 \right] \omega \, . \tag{35}$$

The second term inside the square bracket is the nonlinear correction to the nontwist linear oscillator frequency $\omega$ in Eq. (19). Observe that this correction is proportional to $\lambda \sim \alpha^{3/2}$. That is, as $\alpha$ increases, the fixed point $(0, \sqrt{\alpha})$ of the nontwist Hamiltonian moves towards a region of high shear $\partial_A H$, and this induces a larger frequency shift. This frequency shift is unique of the nontwist oscillator, and does not occur in the linearization on non-degenerate (twist) Hamiltonians.

Equation (35) provides a second order correction of the kinetic dipole rotation period in Eq. (21). To compute this correction note that for the initial condition in Eqs. (7)–(8)

$$\lambda = \frac{2}{3\gamma^2 \sigma_x^2 \sigma_u^2} \left(\gamma u_1 \sigma_x \sigma_u + |a_0|\right)^{3/2} , \tag{36}$$

which for the parameter values used in Fig. 1, gives $\lambda = 1.5084$. In the evaluation of $\varepsilon$ in Eqs. (25) we have to take the negative sign of $\sqrt{\alpha}$ because $a(0) = -0.2 < 0$. Doing this, we get $\varepsilon = 0.146$ and $\Omega = 1.566$, which gives $T = 8.64$; a value remarkably close to the period $T = 8.66$ according to the numerical results in Fig. 2. As Fig. 4 shows, there is a very good agreement between the analytic solution in Eq. (33) (circles) and the kinetic numerical solution (solid line), whereas as mentioned before the finite–$N$ result seems to oscillate with a shorter period.

### B. Parametric resonance

According to the previous results, an $N = 2$ dipole rotating in the vicinity of the elliptic fixed point creates a periodic self-consistent field with frequency $\Omega$ given in Eq. (35). Since this frequency is near the linear rotation frequency $\omega$ of the particles, there is the possibility of wave-particle resonance [29]. To explore this, we study here the dynamics of test particles in the mean field of an $N = 2$ symmetric dipole.

Let $q$ denote the spatial coordinate of a test particle. Then, using the fact that for the symmetric dipole $a(t) = a^*(t)$, we have from Eqs. (2) and (17), $\ddot{q} = 2A(\tau) \sin q$, where the dots denote derivative with respect to $\tau$. Approximating $\sin q \approx q$ and using Eqs. (33) and (35), we conclude

$$\frac{d^2q}{d\hat{\tau}^2} + \left[1 + 2\left(\frac{5+9\lambda}{3}\right)\varepsilon^2 - 2\,\varepsilon\,\cos\hat{\tau}\right] q = 0\,, \tag{37}$$

where $\hat{\tau} = \omega\tau$. The stability properties of this Mathieu equation are well-understood. In particular, the equilibrium solution $(q, dq/d\hat{\tau}) = (0,0)$ is stable if $\lambda > 5/9$ and unstable if $\lambda < 5/9$, see for example Ref. [30]. Using the definitions of $\lambda$ and $\alpha$, we can write this stability condition in terms of the momentum $\mathcal{P}$ and $\Gamma$ as follows:

$$\mathcal{P} > \left(\frac{5\,\Gamma^2}{6}\right)^{2/3} \quad \text{Stable}\,, \qquad \mathcal{P} < \left(\frac{5\,\Gamma^2}{6}\right)^{2/3} \quad \text{Unstable}\,. \tag{38}$$

In terms of $\alpha$, the origin is stable if $\alpha > \alpha_b$, and unstable if $\alpha < \alpha_b$, where $\alpha_b = (5/6)^{2/3} = 0.8855$ is the bifurcation point. Figure 6 shows the bifurcation of the stability of the $(\pi, 0)$ fixed point in the $(q, \dot{q})$ Poincare section of the test particle dynamics, $\ddot{q} = 2A(\tau)\,\sin q$, in the mean field $A(\tau)$ of a symmetric $N = 2$ dipole for three values of $\alpha$.

These results provide an intuitive understanding of the coexistence of phase space dipoles and Hamiltonian chaos in kinetic and many-particles simulations like those in Figs. 1 and 3. In particular, a natural next step in the macroparticle simplification of the dipole described in Sec. II, is to model the dipole as to two macroparticles surrounded by a "cloud" of particles which in a first approximation do not interact. This non-interacting (test particle) assumption is reasonable provided the particle concentration in the cloud is small compared to the particle concentration in the "core" of the dipole. The two upper panels in Fig. 7 show contour plots of the instantaneous position of the dipole in Fig. 1. As the dipole rotates, it creates a self-consistent mean field, which, as shown in Fig. 2, is periodic in time. The time dependence of $a(t)$ manifests in the "breathing" of the separatrix and explains the chaos observed in the test–particle Poincare sections shown in the lower two panels of Fig. 7. The mean field–dipole resonance creates two islands of integrability that contain the hole and clump forming the dipole. In this case the $(\pi, 0)$ fixed point is stable, a result consistent with the fact that according to Eq. (36), $\lambda = 1.501 > 5/9$.

## IV. ELLIPTIC–HYPERBOLIC BIFURCATION

As discussed in the previous section, the hole-clump dipole can maintain its coherence in the presence of a time-dependent mean field. However, this is not always the case, and an important problem is to know how and when dipolar structures lose their coherence. Chaotic transport certainly plays an important role in the destruction and eventual mixing of phase space structures. In particular, dipole initial conditions with large values of $\Gamma_j$ induce large variations in the mean field amplitude and typically result in widespread chaotic mixing. However, in addition to chaotic transport, the single wave model exhibits another transport mechanism that leads to phase space mixing. The goal of this section is to discuss this transport mechanism.

Panel (a) in Fig. 8 shows the initial condition in Eq. (7) consisting of two symmetric Gaussian-distributed holes and clumps with $\gamma = 12$, $x_1 = \pi$, $x_2 = \pi$ and $u_1 = -u_2 = -0.4$, and $a_0 = -0.36$. This is the same initial condition as the one used in Fig. 1 except that the value of $\gamma$ has been increased. Note also that the dipole in Fig. 8 (a) is rotated by $\pi$, and that there is a corresponding phase shift in $a(t)$. At the beginning the dipole rotates around $(x, y) = (\pi, 0)$, but eventually it loses coherence by filamenting into very small scale structures difficult to resolve numerically. At this point it is more convenient to resort to finite–$N$ particle simulations like the one in Fig. 9. In this simulation the initial condition of the mean field was $a_0 = -0.36$, and the particles initial condition, shown in Fig. 9 (a), consisted of an $N = 1000$ discretization of the continuous distribution function in Fig. 8 (a) with the same energy and momentum. In this case it is observed that the dipole filamentation due to the elliptic–hyperbolic bifurcation, is followed by the chaotic mixing of the holes and clumps in the stochastic layer of the mean field.

To understand these numerical results we resort once more to the $N = 2$ macroparticle description. According to Eq. (2), the Hamiltonian of the symmetric hole–clump system is $H(x_j, u_j, t) = \sum_j u_j^2/2 + 2a(t) \sin x_j$. This Hamiltonian has two fixed points: $(x_j, u_j) = (0, 0)$ and $(\pi, 0)$, and the stability of these fixed points is determined by the sign of $A = a\Gamma^{-2/3}$.

If $A > 0$, then $(0,0)$ is elliptic and $(\pi,0)$ is hyperbolic. However, if $A < 0$, then $(0,0)$ is hyperbolic and $(\pi,0)$ is elliptic. Accordingly, a change in time of the sign of $A$ is accompanied with an elliptic–hyperbolic bifurcation. As shown in Figs. 5(a) (b), a fraction of the orbits in the $(x,A)$–space experiences a change of sign in $A$ while crossing the dashed line $A = 0$. For a given initial condition $(x_0, A_0)$, there will be elliptic–hyperbolic bifurcations provided

$$-1 < \alpha\, A_0 - \frac{A_0^3}{3} + \cos x_0 < 1\,. \tag{39}$$

This condition follows from the fact that at the bifurcation point $(x,A) = (x_b, 0)$ , $H = \alpha A_0 - A_0^3/3 + \cos x_0 = \cos x_b$. Assuming $x_0 = 0$ and using the definition of $\alpha$ in (17), we have the following condition for the bifurcation in terms of the initial conditions $a_0 = a(0)$, $u_0 = u(0)$ and $\Gamma$

$$-6\,\Gamma^2 < 3\,\Gamma u_0\, a_0 + 2\, a_0^3 < 0\,. \tag{40}$$

Figure 10 shows a plot of this condition in the $(a_0, u_0)$ parameter space.

Figure 11 shows an example of an elliptic–hyperbolic bifurcation in a numerical integration of Eqs. (1)–(3) for one hole and one clump, $N = 2$. The empty (full) circle denotes the instantaneous $(x,u)$ position of the hole (clump) along its path plotted with a dashed (solid) curve. The figure also shows the instantaneous position of the separatrix of the Hamiltonian $H = u^2/2 + 2a\sin x$. In both cases $\Gamma_1 = -\Gamma_2 = 1$, and $U = 0$. The various panels display the state of the system at successive instants of time. The initial conditions at $t = 0$ are $(x_0, u_0) = (0, 0.25)$ and $a_0 = -0.5$. In the rescaled variables, they correspond to $A_0 = -0.5$, and $\alpha = 0.5$ which are the initial conditions used in the trapped, hole-clump state in the homoclinic topology in Fig. 5–(a). At $t = 3.94$ (first panel), $A > 0$, and the hole-clump pair is trapped inside the wave separatrix. At $t = 6.0745$ (third panel), $A$ vanishes, and following this an hyperbolic point forms at the origin. The hole-clump pair moves along the stable and unstable manifolds of the hyperbolic fixed point until $t = 9.71851$ when $A$ vanishes again, and an elliptic forms at the origin. This sequence repeats periodically in time. It is also possible to have an elliptic–hyperbolic bifurcation for an untrapped hole-clump state.

These results provide an explanation of the dipole destruction in Figs. 8 and 9. According to Eqs. (20) and (21), the total momentum and effective $\Gamma$ in this case are $\mathcal{P} = -0.2256$ and $\Gamma = 0.24$. With $a_0 = -0.36$ and $x_0 = \pi$, it is seen that the inequality in Eq. (39) is satisfied ($-1 < 0.68 < 1$) implying that the initial condition will develop an elliptic–hyperbolic bifurcation. Figure 12 shows the evolution of the dipole in Fig. 8 along with the evolution of the separatrix. As the dipole rotates, the amplitude of the mean field becomes small and eventually vanishes. The vanishing of the mean field amplitude is accompanied with a jump in phase of the mean field by $\pi$. This, as panel (c) of Fig. 12 shows, leads to the creation of an hyperbolic point at $(\pi, 0)$ that tears the dipole.

## V. SUMMARY AND CONCLUSIONS

Understanding the coexistence of coherent structures and self-consistent Hamiltonian chaos is a nonlinear dynamics problem of relevance to fluid dynamics, plasma physics, galactic dynamics, and statistical mechanics. Two-dimensional, incompressible fluids and plasmas are known to develop large–scale coherent structures that live in a turbulent background. Another example is clustering in phase space, usually observed in models of long–range interacting systems. From the Lagrangian point of view, the problem is to explain the self-consistent formation of islands of integrability that shield the coherent structures from the chaotic mixing of the background. In this paper we have addressed this problem in the context of the single wave model.

The single wave model is a mean field Hamiltonian model in which interacting particles are treated as independent particles moving in an average effective potential determined self-consistently from the motion of all the particles. This model has its origins in the study of the beam-plasma instability, but recently, its range of applicability has been considerably extended to include a wider class of plasma instabilities. The model also describes the dynamics of marginally stable shear flows, and bears similarities with models used in the study of globally coupled rotators in statistical mechanics. From the dynamical systems

perspective, the model is a useful laboratory to study chaos in Hamiltonian systems with many degrees of freedom.

We focused on the study of dipole states consisting of one clump and one hole that correspond to excesses and depletions in the phase space distribution function. Numerical solutions in the kinetic ($N \to \infty$) limit and in the finite–$N$ case, indicate that, depending on the initial conditions, the dipole rotates as a coherent structure or it is destroyed by an elliptic–hyperbolic phase space bifurcation.

To explain these results we treated the dipole as two macroparticles and considered the $N = 2$ limit of the model. In this case the single wave model Hamiltonian has three degrees of freedom (one degree of freedom for the hole, one for the clump, and one for the mean field), and the phase space is six-dimensional. However, symmetry considerations and conservation of linear momentum allows the integrability of the problem by reducing the systems to a one-degree-of-freedom nontwist Hamiltonian. We presented a perturbative analysis of the nontwist Hamiltonian oscillator and observed that there is a self-consistent parametric resonance between the rotation frequency of the dipole and the oscillation frequency of the mean field. This resonance creates islands of stability that shield the hole and the clump from the chaotic transport of the background. Depending on the parameter values and the initial condition, the rotation of the dipole is interrupted by an elliptic–hyperbolic bifurcation in which the amplitude of the mean field vanishes and its phase jumps by $\pi$. This bifurcation tears the dipole and eventually leads to the rapid mixing of the distribution function in phase space.

We restricted attention to trapped dipole states. However, there are also untrapped dipole states consisting of one hole and one clump located above and below the separatrix. These untrapped dipoles also exhibit an elliptic–hyperbolic bifurcation. The integrability of the $N = 2$ system, and to some degree the robustness of the dipole states, depend on the hole-clump symmetry, $(x, u, f, a) \to (-x + 2\pi, -u, -f, a^*)$, and an open problem is to study the dynamics of coherent structures when this symmetry is broken. Another problem of interest is to explore the role of the elliptic–hyperbolic bifurcation in the time evolution

of general initial conditions. Numerical simulations show the existence of rapid relaxation of far from equilibrium initial condition due to "violent" mixing driven by successive elliptic–hyperbolic bifurcations.

**Acknowledgments**

The authors acknowledge useful conversations with Yves Elskens, Francois Leyvraz, Stefano Ruffo, and Andrea Rapisarda. MCF is very grateful to the plasma theory group at the Oak Ridge National Laboratory for its hospitality, and thanks the European Commission for support through a Marie Curie individual fellowship contract No HPMFCT-2000-00596. This work was sponsored by the Oak Ridge National Laboratory, managed by UT-Battelle, LLC, for the U.S. Dept. of Energy under contract DE-AC05-00OR22725.

# REFERENCES


[1] A. Crisanti, M. Falcioni, G. Paladin, and A. Vulpiani, La Rivista del Nuovo Cimento **14**, 1 (1991).

[2] D. del-Castillo-Negrete, CHAOS **10**, 75-88 (2000).

[3] D. del-Castillo-Negrete, Physica A **280**, 10-21 (2000).

[4] T. M. O'Neil, J. H. Winfrey, and J. H. Malmberg, Phys. Fluids **14**, 1204 (1971).

[5] I. N. Onischenko *et al.*, JETP Lett. **12**, 281 (1970).

[6] J. L. Tennyson, J. D. Meiss, and P. J. Morrison, Physica D **71**, 1 (1994).

[7] M. Antoni, Y. Elskens, and D. F. Escande, Phys. Plasmas **5**, 841 (1998).

[8] D. del-Castillo-Negrete, Phys. Letters A **241**, 99-104 (1998).

[9] D. del-Castillo-Negrete, Physics of Plasmas **5**, 3886 (1998).

[10] D. Farina, F. Casagrande, U. Colombo, and R. Pozzoli, Phys. Rev. E **49**, 1603-1609 (1994).

[11] N. J. Balmforth, S. L. Smith, and W. R. Young, J. Fluid Mech. **426**, 95-133 (2001).

[12] S. M. Churilov and I. G. Shukhman, J. Fluid Mech. **318**, 189 (1996).

[13] M. E. Goldstein and L. S. Hultgren, J. Fluid Mech., **197**, 295 (1988).

[14] N. J. Balmforth and C. Piccolo, J. Fluid Mech. **449**, 85-114 (2001).

[15] M. Antoni and S. Ruffo, Phys. Rev. E **52**, 2361 (1995).

[16] V. Latora, A. Rapisarda, and S. Ruffo, Physica D **131**, 38 (1999).

[17] H. L. Berk, B. N. Breizman, and N. V. Petviashvili, Phys. Letters A **234**, 213-218 (1997).

[18] D. A. Schecter and D. Dubin, Phys. Rev. Letters, **83**, 2191-2194 (1999).

[19] A. Provenzale, Annu. Rev. Fluid Mech. **31**, 55-93 (1999).

[20] D. A. Schecter, D. H. E. Dubin, K. S. Fine, and C. F. Driscoll, Phys. Fluids **11**, 905-914, (1999).

[21] J. Barre, T. Dauxois, and S. Ruffo, Physica A **295**, 254-60 (2001).

[22] C. Z. Cheng and G. Korr, J. Comp. Phys. **22**, 330-351 (1976).

[23] M.-C. Firpo and Y. Elskens, Journal of Statistical Physics **93**, 193-209 (1998).

[24] F. Doveil, M.-C. Firpo, Y. Elskens, D. Guyomarc'h, M. Poleni and P. Bertrand, Physics Letters A **284**, 279-285 (2001).

[25] M.-C. Firpo, F. Doveil, Y. Elskens, P. Bertrand, M. Poleni and D. Guyomarc'h, Physical Review E **64**, 026407 (2001).

[26] J. R. Cary and I. Doxas, J. Comput. Phys. **107**, 98 (1993); I. Doxas and J. R. Cary, Phys. Plasmas **4**, 2508 (1997).

[27] D. del-Castillo-Negrete, J. M. Greene, and P. J. Morrison, Physica D **91**, 1 (1996).

[28] D. del-Castillo-Negrete and J. M. Morrison, Phys. Fluids A **5**, 948 (1993).

[29] G. P. Berman and G. M. Zaslavsky, Sov. J. Plasma Phys. **3** (6), 744-749 (1977).

[30] E. J. Hinch, *Perturbation methods*, (Cambrdige University Press, New York, 1991).

## FIGURE CAPTIONS

FIG. 1. Kinetic simulation, $N \to \infty$, of a rotating dipole obtained from the numerical integration of Eqs. (4)–(5) with initial condition in Eqs. (7)–(8). Red corresponds to $f > 0$ (clump) and blue to $f < 0$ (hole). The panels show the dipole at $t = 0, \Delta, 2\Delta, \ldots 7\Delta$, where $\Delta = 1.237$ and $7\Delta = 8.66$ is the rotation period of the dipole. Figure 3 shows the corresponding finite–$N$ numerical simulation, and Fig. 2 the mean field $a(t)$.

FIG. 2. Real part of mean field $a$ as function of time corresponding to the coherent rotating dipole solution shown in Fig. 1. In this case, the imaginary part of $a$ vanishes identically for all $t$.

FIG. 3. Finite–$N$ discrete particle simulation of rotating dipole obtained from the numerical integration of Eqs. (1)–(3). The initial condition consisted of a finite–$N$ discretization of $f(x, u, t = 0)$ in Eq. (7) with $N = 1000$ particle, half of them clumps and the other half holes. The red dots denote clumps and blue dots holes. The panels show the dipole at $t = 0, \Delta_N, 2\Delta_N, \ldots 7\Delta_N$, where $\Delta_N = 1.1793$ and $7\Delta_N = 8.255$ is the rotation period of the dipole. Figure 1 shows the corresponding $N \to \infty$ kinetic simulation, and Fig. 4 the mean field $a(t)$.

FIG. 4. Mean field $a$ as function of time over one period of the dipole oscillation. The solid curve is the result from the kinetic simulation in Fig. 1, and the dashed line is the finite–$N$ discrete particle simulation in Fig. 3. The circles correspond to the second order perturbative solution in Eq. (33).

FIG. 5. Contour plots of the symmetric dipole, reduced Hamiltonian in Eq. (16) for: (a) $\alpha = 0.5$, and (b) $\alpha = 1.95$. Case (a) shows the homoclinic topology and case (b) the heteroclinic topology. Orbits crossing the dashed line $A = 0$ give rise to elliptic–hyperbolic bifurcations like the ones shown in Fig. 11.

FIG. 6. Poincare sections in the $(q, \dot{q})$ –plane of the test particle dynamics, $\ddot{q} = 2A(\tau) \sin q$, with $A$ given by the perturbative analytical solution in Eq. (33) with $\varepsilon = 0.1$ and three values of $\alpha$. In (a) $\alpha = 2$, and in (c) $\alpha = 0.2$. Panel (b) corresponds to the bifurcation point $\alpha = \alpha_b = (5/6)^{2/3} = 0.8855$ according to Eq.(38).

FIG. 7. The two panels on the top show contour plots of the rotating dipole solution in Fig. 1 at two successive times $t = 4.949$, and $t = 7.423$. Also shown are the instantaneous contour lines of the Hamiltonian in Eq. (2), with the sparatrix shown in red. The two panels on the bottom show Poincare sections for test particles in the mean field of the rotating dipole solution in Fig. 1.

FIG. 8. Dipole destruction through an elliptic–hyperbolic bifurcation in the $N \to \infty$ kinetic limit according to the numerical integration of Eqs. (4)–(5) for the initial condition in Eq. (7) with $\gamma = 12$, $x_1 = x_2 = \pi$, $u_1 = -u_2 = -0.4$, $a_0 = -0.36$, $\sigma_x = 0.2$, $\sigma_u = 0.1$, and $U = 0$. Red corresponds to $f > 0$ (clump), and blue to $f < 0$ (hole).

FIG. 9. Dipole destruction through an elliptic–hyperbolic bifurcation, and phase space mixing in the finite–$N$ discrete particle case. Solution obtained from the numerical integration of Eqs. (1)–(3), with initial condition corresponding to an $N = 1000$ discretization of the continuous initial condition $f(x, u, t = 0)$ used in Fig. 8. Red dots correspond to clumps and blue dots to holes. The panels show the phase space at $t = 0$, 2.26, 3.89, 6.35, 11.91, 23.81, 31.75, and 39.69. The elliptic–hyperbolic bifurcation occurs at $t = 3.866$.

FIG. 10. Elliptic–hyperbolic bifurcation diagram for $\Gamma = 1$. According to Eq. (40), when $x_0 = x(0) = 0$, there is an elliptic–hyperbolic bifurcation for initial conditions in the shaded region. The shape of the shaded region for other values of $\Gamma$ is qualitatively the same.

FIG. 11. Elliptic–hyperbolic bifurcation generated by a symmetric, hole-clump pair. Each panel shows the instantaneous positions of the hole (empty circle) and clump (full

circle), the trajectories of the hole (dashed curve) and clump (solid curve), and the instantaneous wave separatrix, at successive times. The third and seventh panels show the elliptic–hyperbolic bifurcations. This pattern repeats periodically in time.

FIG. 12. Elliptic–hyperbolic bifurcation and dipole destruction. The first five panels show contour plots of the destruction of a dipole. Also shown are contour plots of the instantaneous single wave model Hamiltonian in Eq. (2), with separatrix shown in red. The last panel shows the wave amplitude $\rho = |a|$ as function of time, with the dots showing the times corresponding to the contour plots. The vanishing of $\rho$ around $t \sim 6$ signals the onset of the elliptic–hyperbolic bifurcation.

FIGURES

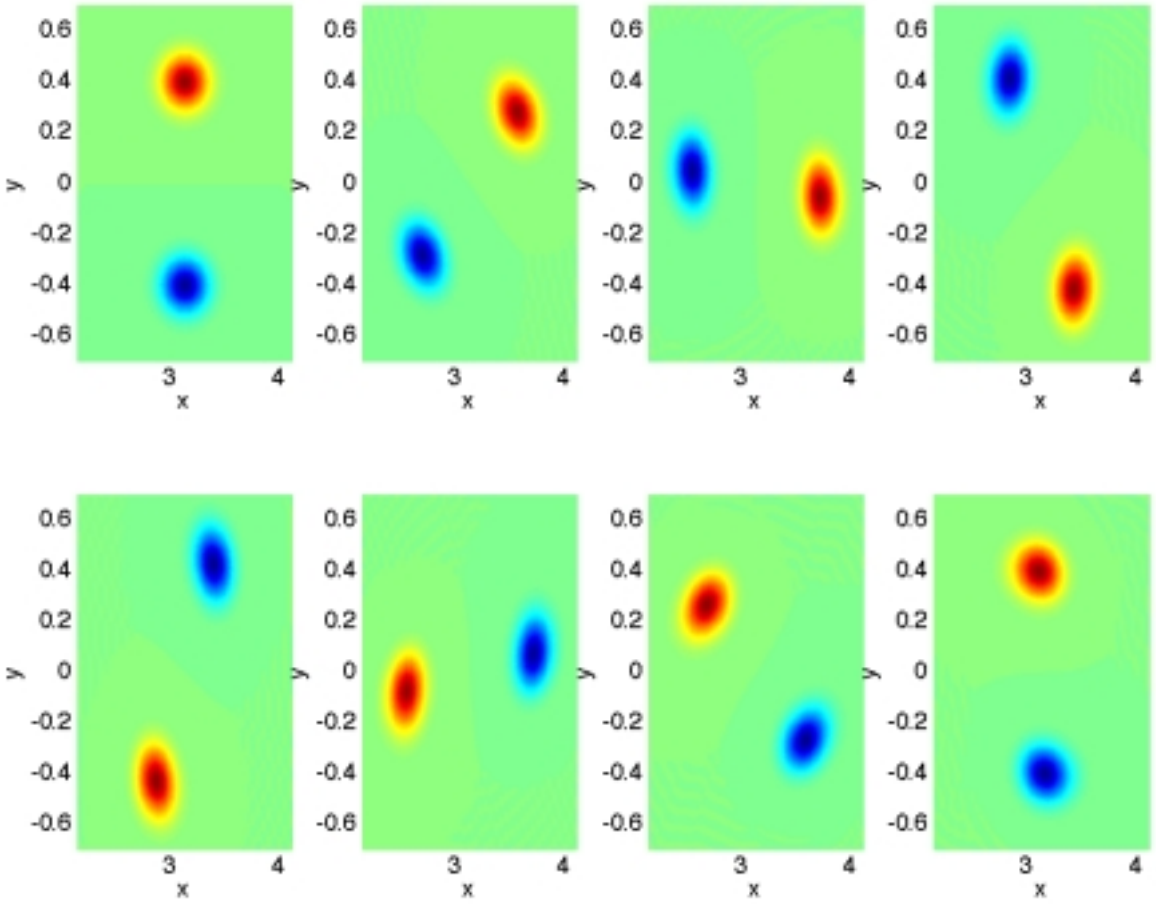


FIG. 1.

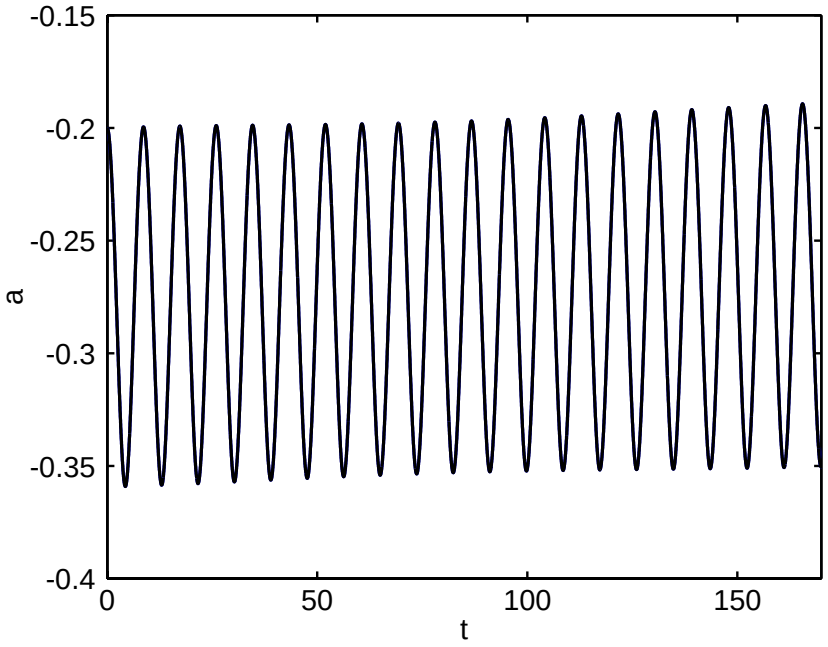

FIG. 2.

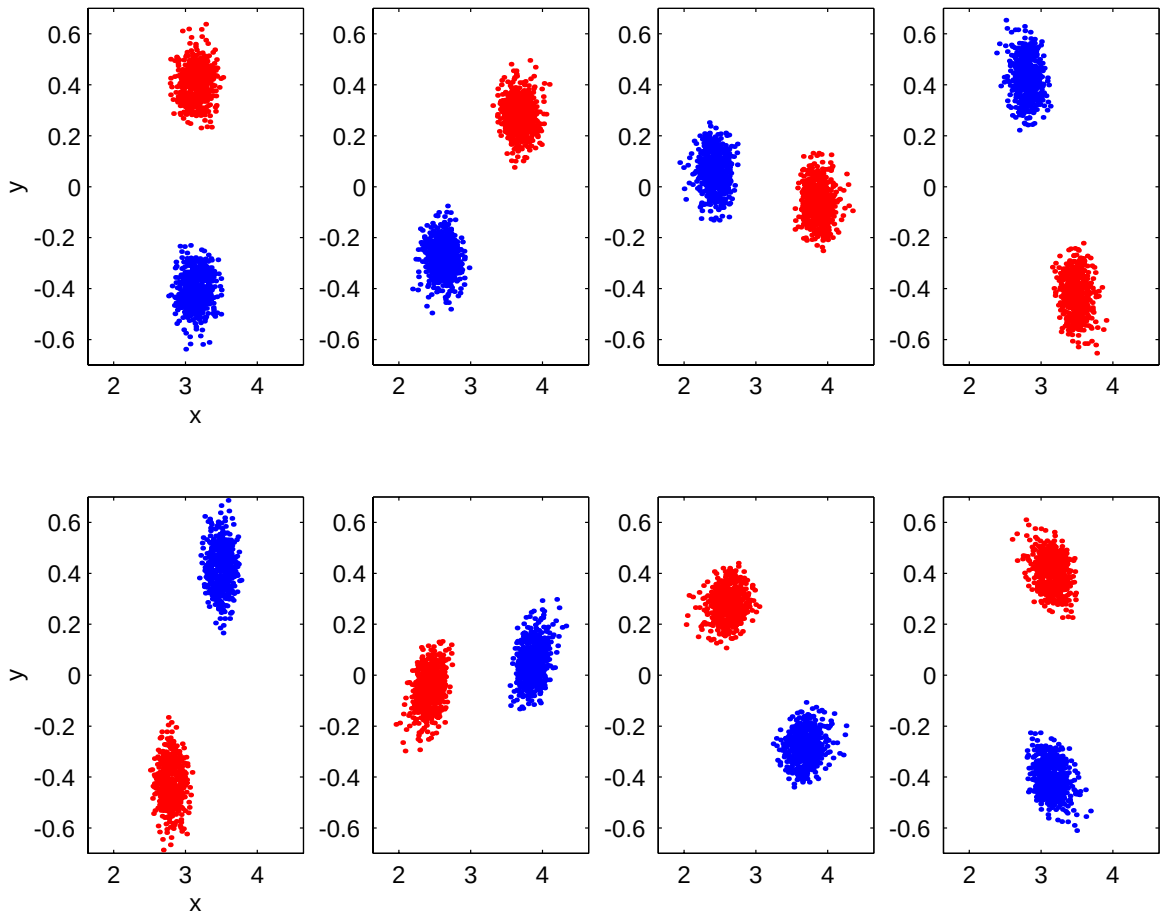


FIG. 3.

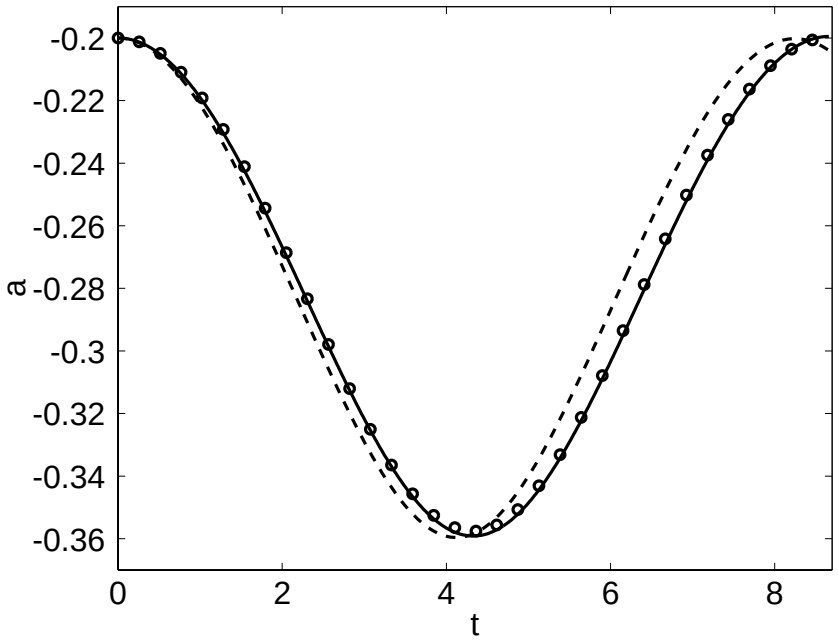

FIG. 4.

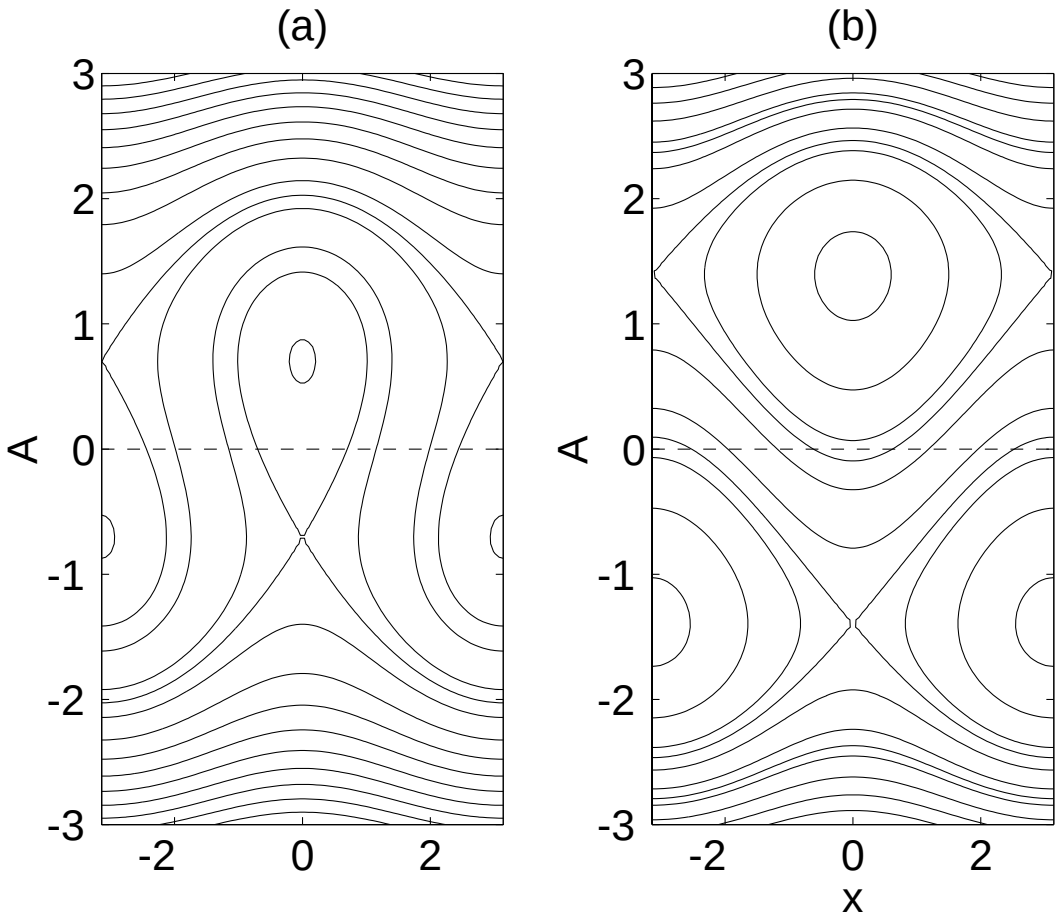


FIG. 5.

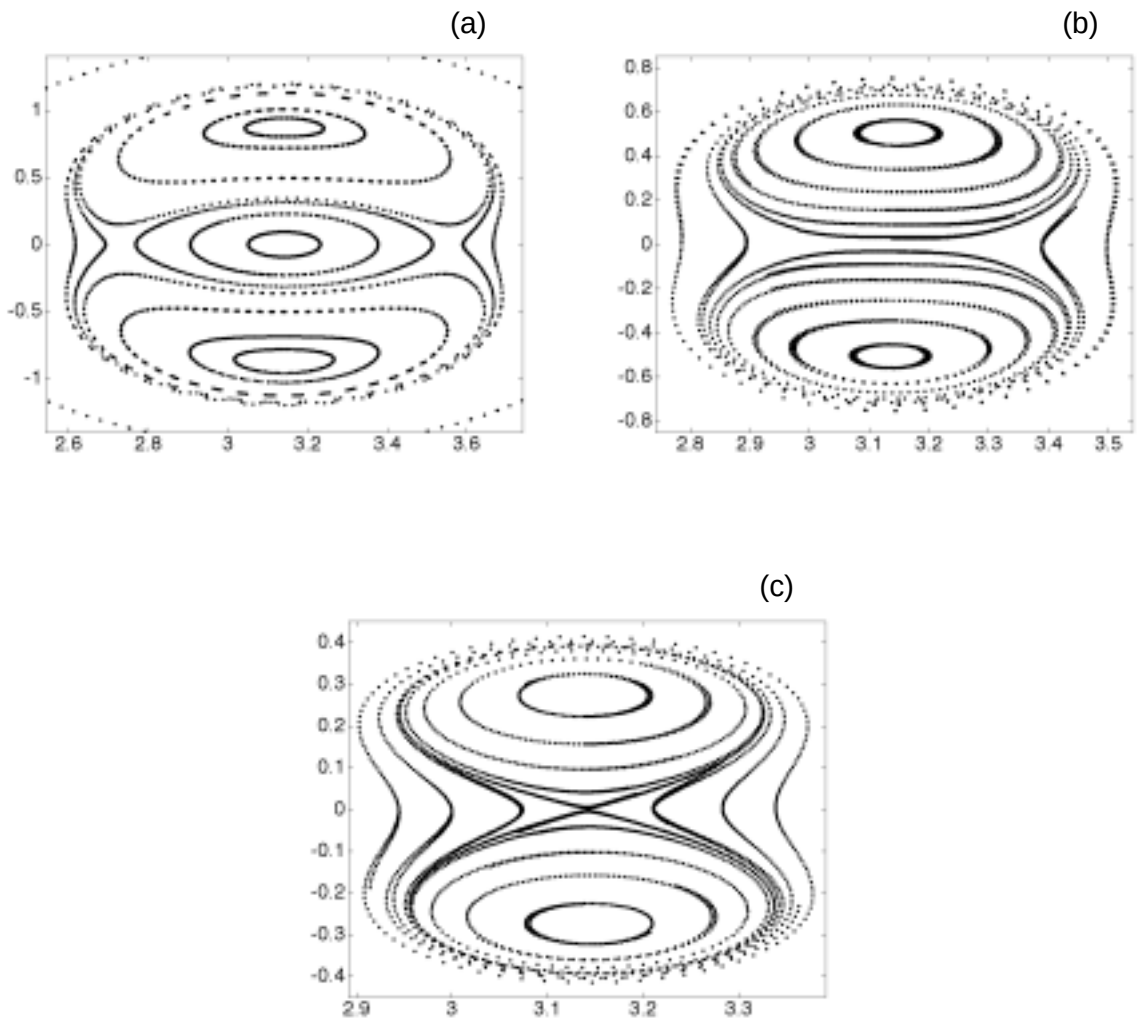


FIG. 6.

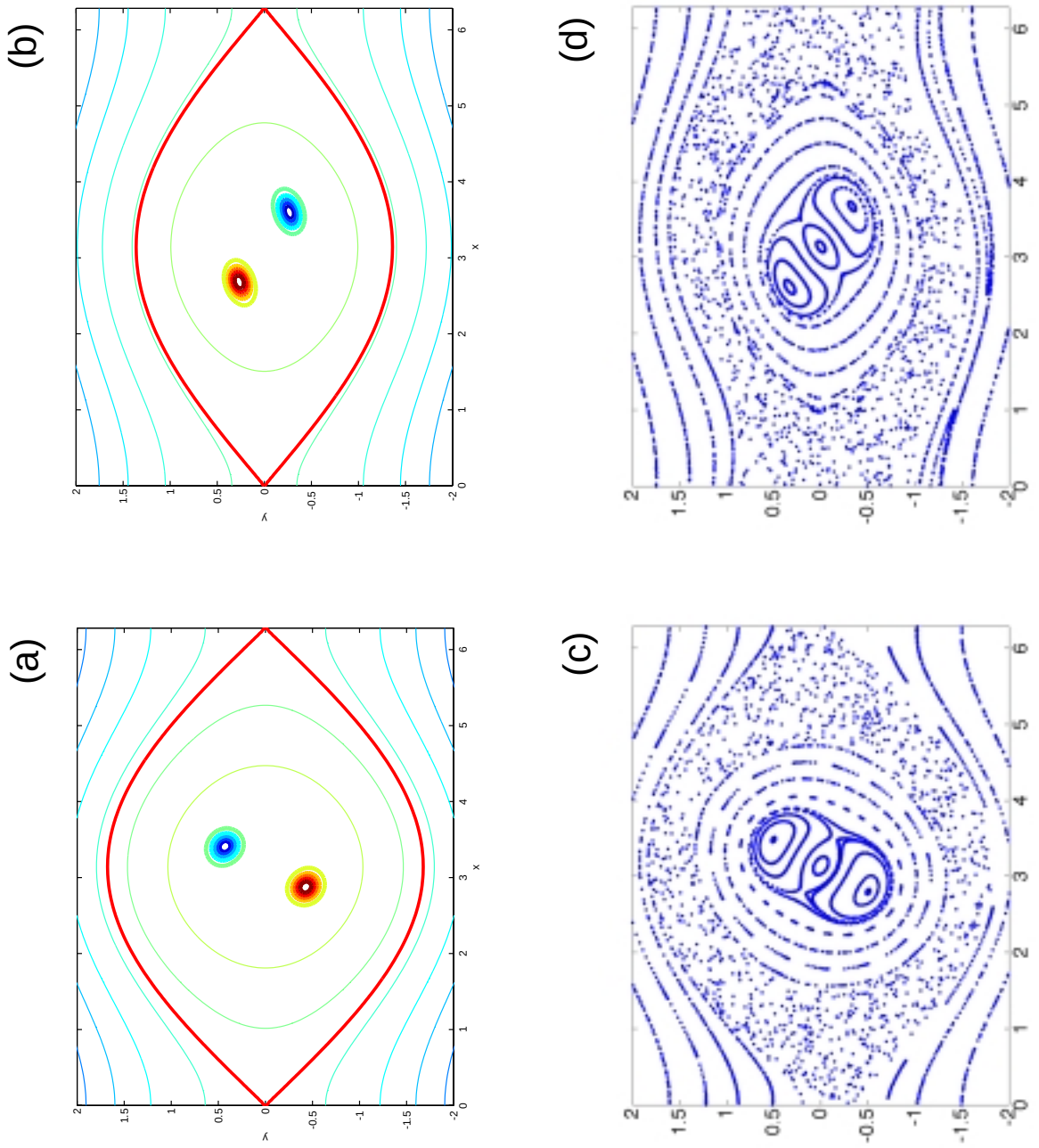


FIG. 7.

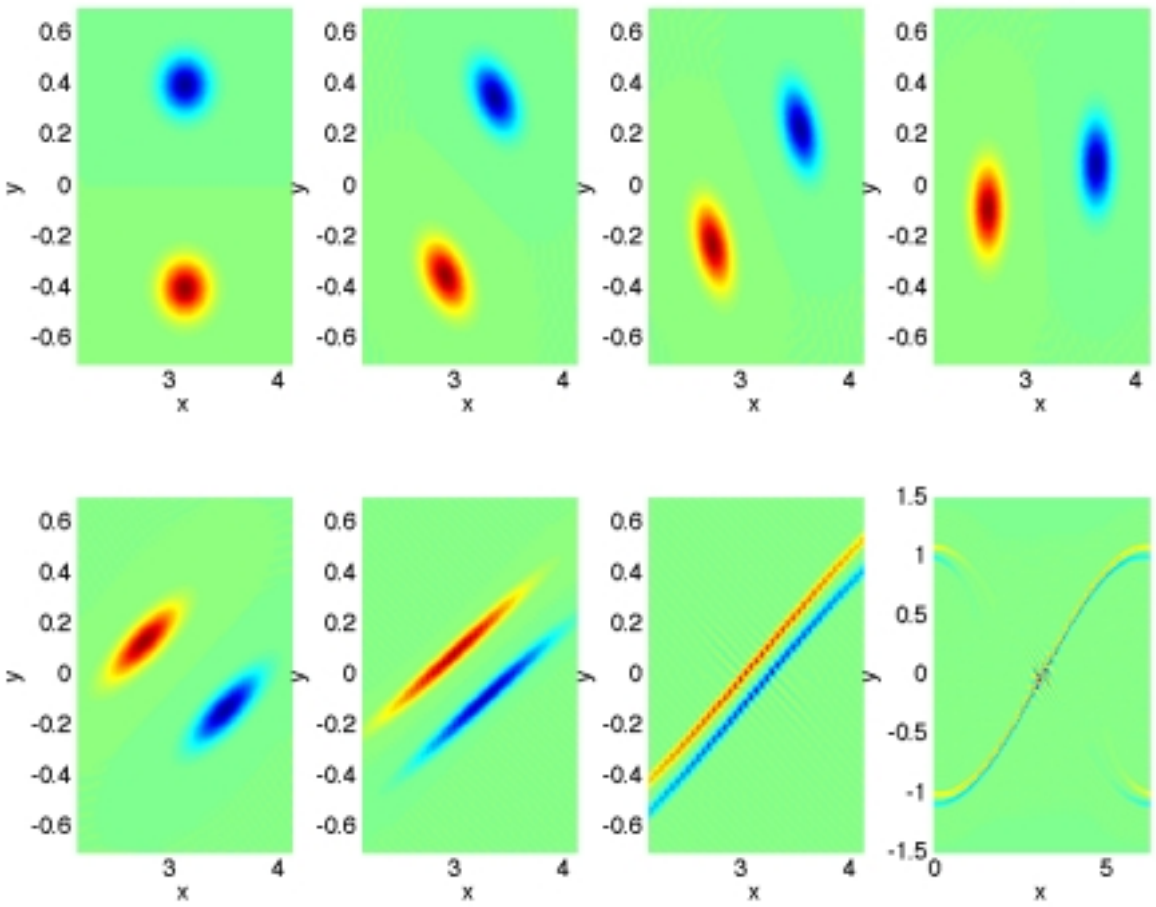


FIG. 8.

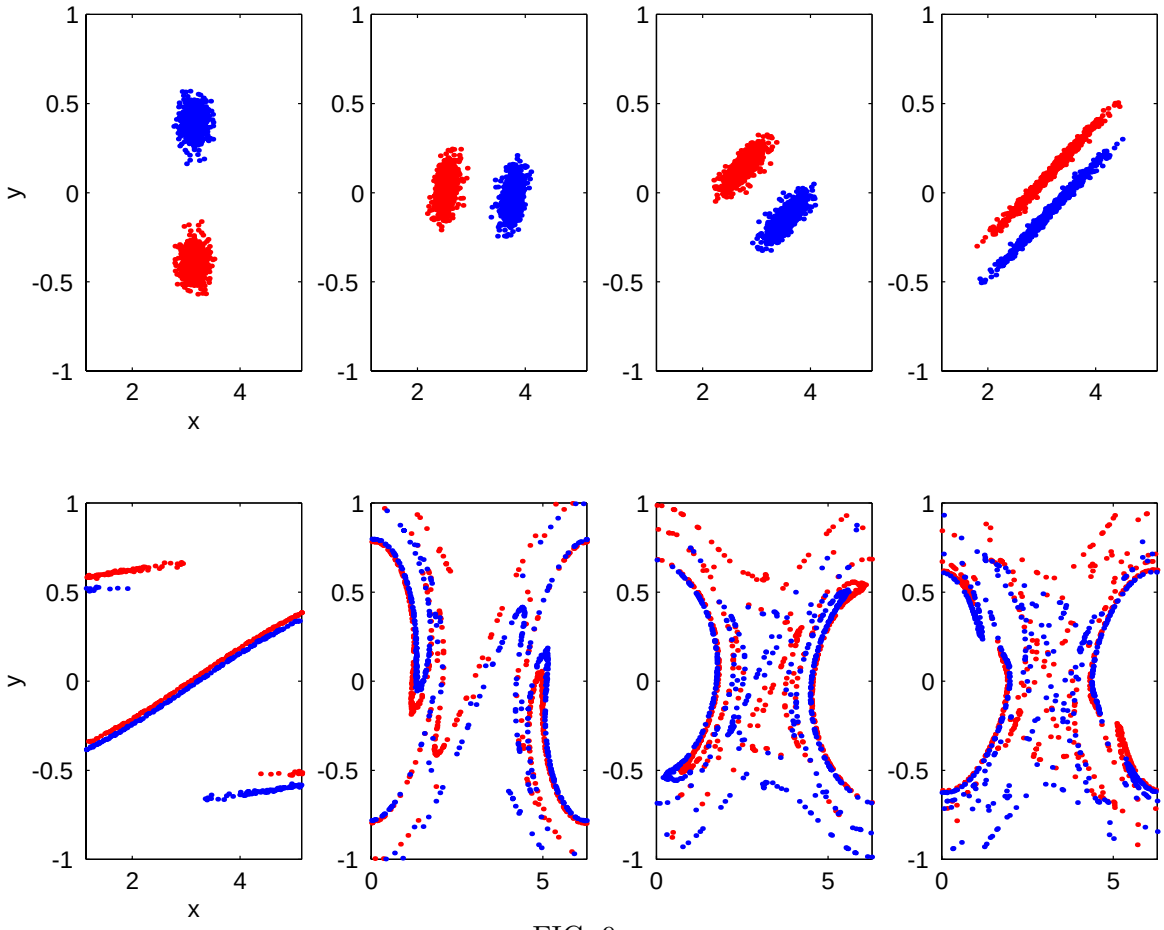


FIG. 9.

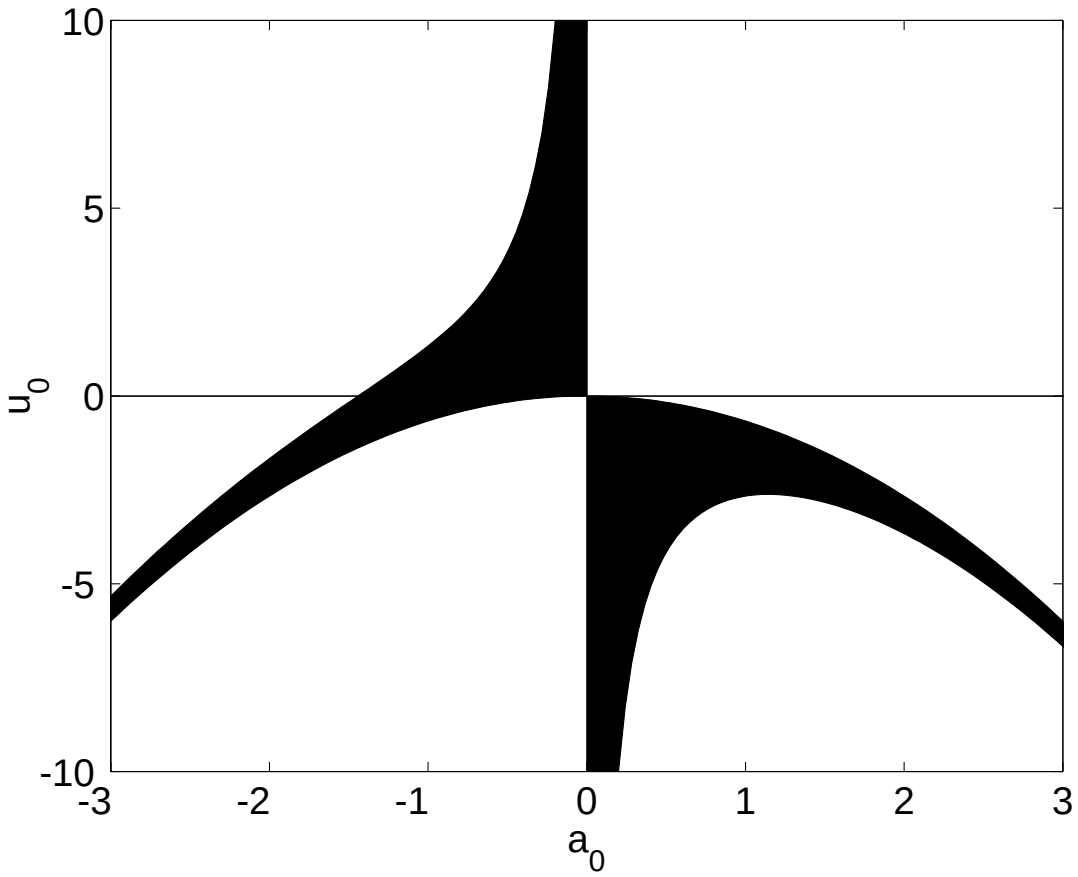

FIG. 10.

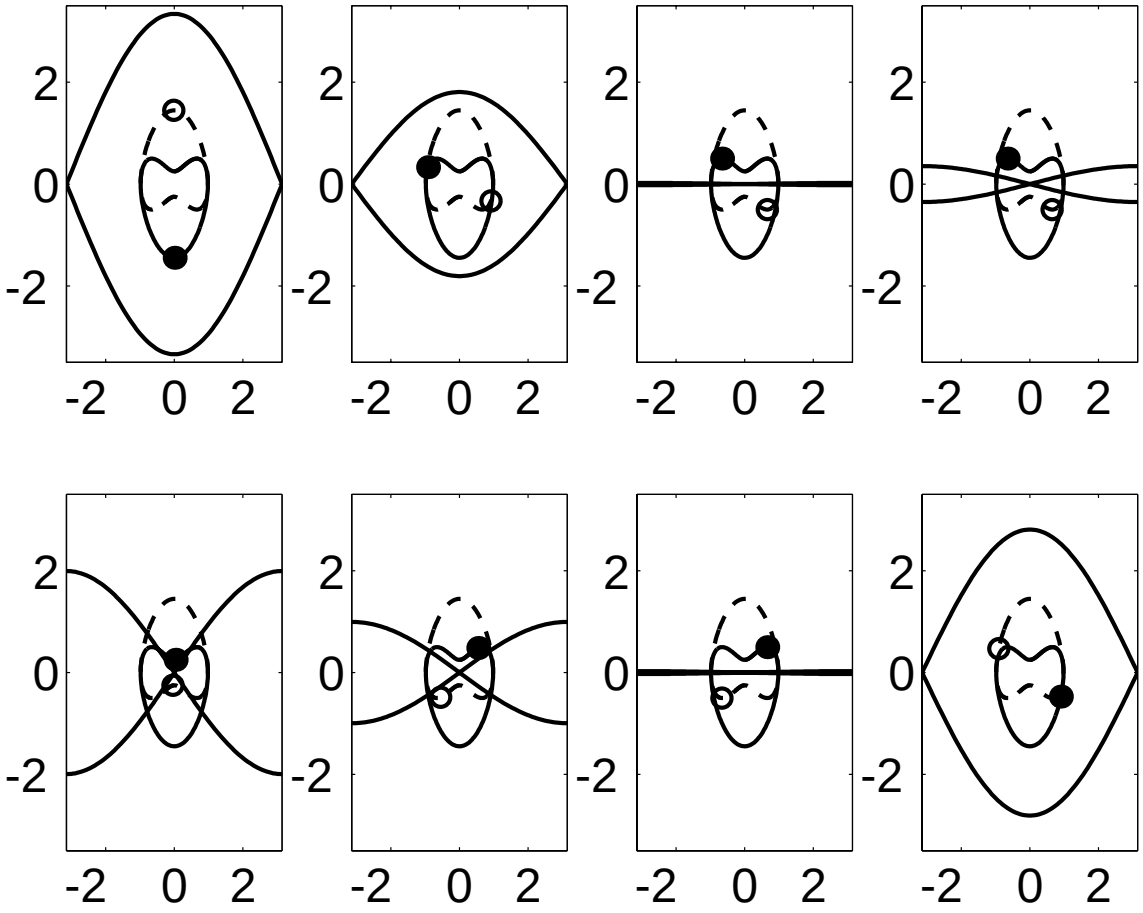

FIG. 11.

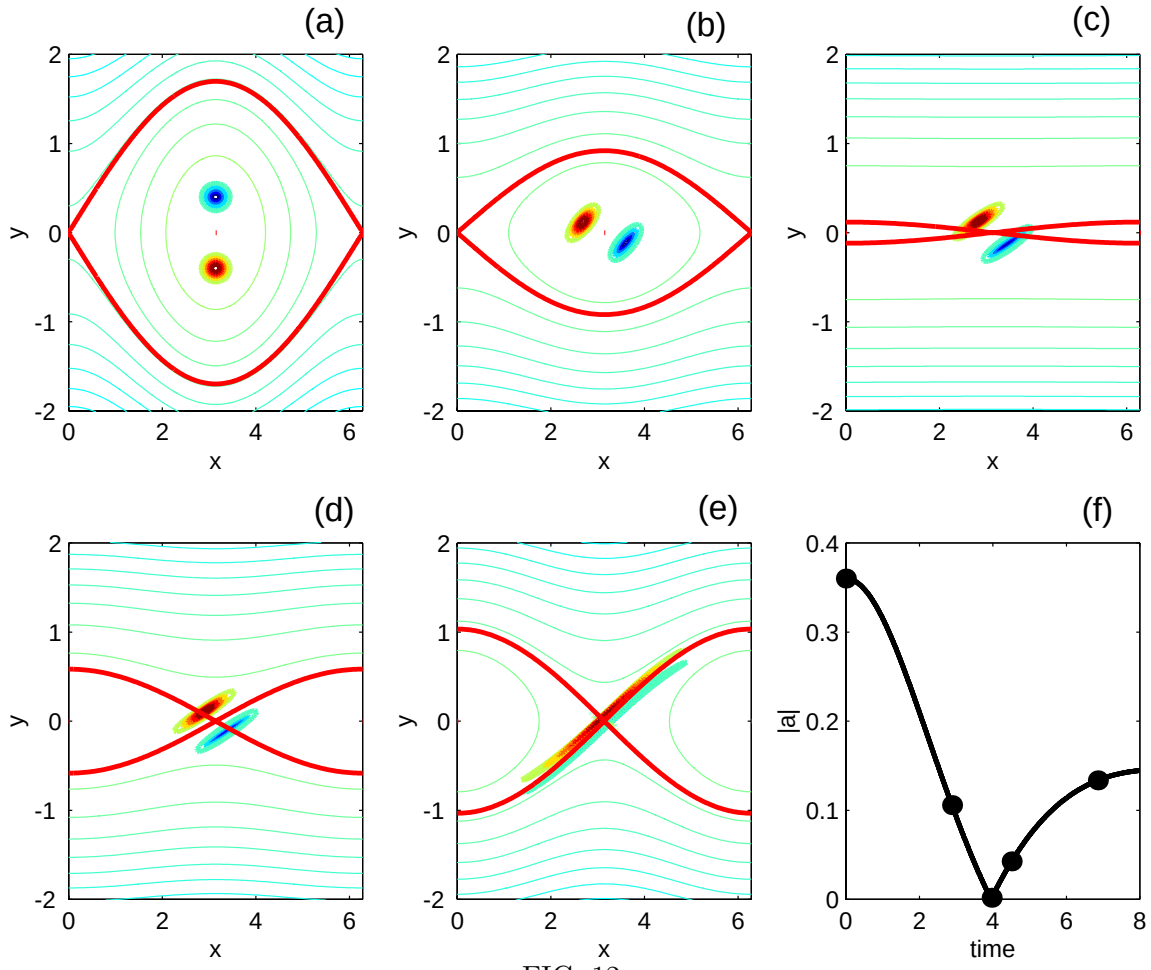

FIG. 12.